Permanent Densification of Calcium Aluminophosphate Glasses

Kapoor, Saurabh; Youngman, Randall E.; Ma, Lina; Lönnroth, Nadja; Rzoska, Sylwester J.; Bockowski, Michal; Jensen, Lars Rosgaard; Bauchy, Mathieu; Smedskjær, Morten Mattrup

Published in:
Frontiers in Materials

DOI (link to publication from Publisher):
10.3389/fmats.2019.00063

Publication date:
2019

Document Version
Publisher's PDF, also known as Version of record

frontiers in Materials

ORIGINAL RESEARCH
published: 18 April 2019
doi: 10.3389/fmats.2019.00063

Permanent Densification of Calcium Aluminophosphate Glasses

Saurabh Kapoor[1], Randall E. Youngman[2], Lina Ma[2], Nadja Lönnroth[2], Sylwester J. Rzoska[3], Michal Bockowski[3], Lars R. Jensen[4], Mathieu Bauchy[5] and Morten M. Smedskjaer[1]**

[1] Department of Chemistry and Bioscience, Aalborg University, Aalborg, Denmark, [2] Science and Technology Division, Corning Incorporated, Corning, NY, United States, [3] Institute of High-Pressure Physics, Polish Academy of Sciences, Warsaw, Poland, [4] Department of Materials and Production, Aalborg University, Aalborg, Denmark, [5] Department of Civil and Environmental Engineering, University of California, Los Angeles, Los Angeles, CA, United States

High-temperature densification of oxide glasses influences their interatomic distances and bonding patterns, resulting in changes in the mechanical and chemical properties. Most high-pressure investigations have focused on aluminosilicate and aluminoborosilicate based glasses, due to their relevance for the glass industry as well as the geological sciences. Relatively few studies have explored the pressure-induced changes in the structure and properties of phosphate-based glasses, although P_2O_5 is an important component in various multicomponent oxide glasses of industrial interest. In this work, we investigate the influence of permanent densification on the structure, mechanical properties (Vicker's hardness), and chemical durability (weight loss in water) of binary CaO-P_2O_5 and ternary CaO-Al_2O_3-P_2O_5 glasses. The densification of bulk glasses is obtained through isostatic compression (1–2 GPa) at the glass transition temperature. The binary CaO-P_2O_5 series is prepared with varying [CaO]/[P_2O_5] ratios to obtain glasses with different O/P ratios, while the ternary series CaO-Al_2O_3-P_2O_5 is prepared with a constant O/P ratio of 3 (metaphosphate) but with varying [CaO]/([CaO]+[Al_2O_3]) ratio. Using Raman and ^{31}P NMR spectroscopy, we observe minor, yet systematic and composition-dependent changes in the phosphate network connectivity upon compression. On the other hand, ^{27}Al NMR analysis of the compressed CaO-Al_2O_3-P_2O_5 glasses highlights an increase in the Al coordination number. We discuss these structural changes in relation to the pressure-induced increase in density, Vicker's hardness, and chemical durability.

Keywords: oxide glass, vickers micro hardness, hot compression, structure-property relationship, chemical durability

OPEN ACCESS

Edited by:
Lothar Wondraczek, Friedrich Schiller University Jena, Germany

Reviewed by:
Dominique De Ligny, University of Erlangen Nuremberg, Germany
Mouritz Nolsøe Svenson, Particle Analytical, Denmark

****Correspondence:***
Saurabh Kapoor
kapoor0588@gmail.com
Morten M. Smedskjaer
mos@bio.aau.dk

Specialty section:
This article was submitted to Glass Science, a section of the journal Frontiers in Materials

Received: *31 January 2019*
Accepted: *27 March 2019*
Published: *18 April 2019*

Citation:
Kapoor S, Youngman RE, Ma L, Lönnroth N, Rzoska SJ, Bockowski M, Jensen LR, Bauchy M and Smedskjaer MM (2019) Permanent Densification of Calcium Aluminophosphate Glasses. Front. Mater. 6:63. doi: 10.3389/fmats.2019.00063

INTRODUCTION

The application of pressure enables tuning of the interatomic distances and bonding patterns in glassy solids (Kapoor et al., 2017c), providing an additional degree of freedom for altering glass properties compared to varying composition or temperature alone. Understanding the gradual or abrupt densification mechanisms involving various structural transitions is thus an important task in glass science and engineering, but it is complicated by the intrinsic atomic-scale disorder in glasses and the experimental difficulties in undertaking *in situ* high-pressure characterization experiments (Huang and Kieffer, 2004). Permanent densification of bulk glasses can be achieved at

a modest pressure (∼1 GPa) by high-temperature compaction, enabling *ex situ* characterization and a controlled extent of densification by the choice of pressure and temperature treatment. Such hot compression treatments may be used as an effective post-treatment method (Kapoor et al., 2018). More generally, understanding the effect of densification on glass structure and properties is important for understanding the fracture mechanics of glasses at the atomic level (Januchta et al., 2017), since stresses in the GPa regime are easily reached during sharp contact deformation (e.g., Vickers indentation). Such deformation is a typical failure mode for, e.g., cover glass applications (Gross, 2012).

Aluminosilicate glasses are currently applied in various technological innovations, including chemically durable, scratch resistant, and high strength glasses for electronic and automobile industries (Ellison and Cornejo, 2010; Kafer et al., 2013). However, an ever-increasing demand for stronger, tougher, and more chemically durable glasses has led to the exploration of oxide glasses containing multiple network formers such as SiO_2, Al_2O_3, P_2O_5, and B_2O_3 (Ellison et al., 2014). The non-silicate network polyhedra interact, often in unpredictable ways, by forming a variety of structural associations, such as Al^{IV}-B^{III}, B^{III}-B^{IV}, Al^{V}, $AlPO_4$, and BPO_4 units (Gan et al., 1994; van Wüllen et al., 1996; Chan et al., 1998, 1999; Zuchner et al., 1998; Muñoz et al., 2006, 2007, 2008). These structural units result in a significant modification of the atomic network topology and related macroscopic properties. However, it is challenging to understand these interactions unambiguously in complex multicomponent oxide glasses. Furthermore, most of the high-pressure investigations have focused on aluminoborosilicate glasses with relevance for the geological sciences (Kapoor et al., 2017c), while only relatively few studies have explored the pressure-induced changes in structure and properties of P_2O_5-containing glasses (Hirao et al., 1991; Mosey et al., 2005; Gauvin et al., 2007, 2013; Yue et al., 2007; Brazhkin et al., 2011, 2014; Premila et al., 2012; Kapoor et al., 2017b; Shi et al., 2018). These previous studies reveal that the response of P_2O_5-based glasses toward high pressure treatment depends on the glass composition and the utilized compression route (e.g., cold vs. hot compression). We recently showed that hot compression of a binary ZnO-P_2O_5 at 1 GPa resulted in a decrease in the phosphate network polymerization degree, which was possibly compensated by an increase in Zn coordination number (Kapoor et al., 2017b). On the other hand, pressure quenched *v*-P_2O_5 did not show any clear evidence of polymerization changes at pressures <7 GPa (Brazhkin et al., 2011). Finally, we note that the recent inclusion of P_2O_5 as a network former in various compositions for damage resistant cover and display glasses (Aitken, 2008; Ellison et al., 2014; Siebers et al., 2014; Gross and Guo, 2015) further strengthens the need to understand the influence of densification on the structure and properties of P_2O_5-based glasses.

In this work, we investigate the structural and property changes upon densification of binary CaO-P_2O_5 and ternary CaO-Al_2O_3-P_2O_5 series of glasses. The former series is prepared with a varying [CaO]/[P_2O_5] ratio to obtain glasses with different O/P ratios, while the latter is prepared with a constant O/P ratio of 3 (metaphosphate) but with a varying [CaO]/([CaO]+[Al_2O_3]) ratio. Permanent densification is achieved using an N_2 gas pressure chamber with a large inner volume, enabling the compression of bulk samples (mm to cm range) at high pressure (up to 2 GPa) and high temperature (in the range of the glass transition temperature, T_g). Permanent here refers to the finding that the glasses remain in their densified state unless they are heated to temperatures around T_g. Structural characterization was carried out using ^{31}P and ^{27}Al magic angle spinning (MAS) nuclear magnetic resonance (NMR) and Raman spectroscopy. To link the trends in atomic-scale structural changes with macroscopic properties, we also determined the density, hardness (through Vickers indentation), and chemical durability (through weight loss measurements in water).

EXPERIMENTAL SECTION

Sample Preparation

Binary CaO-P_2O_5 and ternary CaO-Al_2O_3-P_2O_5 series of glasses were batched from raw materials of phosphoric acid (VWR Scientific, 85–88%), alumina (Almatis, 99.78%), aluminum metaphosphate (BassTech International, >98%), calcium oxide (Avantor, 94.8%), and calcium pyrophosphate (Alfa Aesar, 96%). Batched raw materials were calcined at 400 °C for 12–16 h, then melted in a platinum crucible at 1,100–1,500°C for 2–4 h with an alumina cover. The glass melts were cast into stainless steel molds, and then annealed for 2 h at their estimated T_g. Samples with dimensions of about 10 × 10 × 3 mm^3 were cut and the flats were optically polished. After cutting and grinding, the samples were then reannealed for 30 min at their measured T_g ($10^{12.2}$ Pa s isokom temperature as determined using beam bending viscosity method) to ensure uniform thermal history. The beam bending viscosity method measures the temperature dependence of viscosity in the range from 10^{11} to 10^{13} Pa s, conforming to ASTM C598 standard.

Ethanol was used for the initial stages of grinding and polishing, using silicon carbide papers of grit size up to 4,000. For the final steps of polishing, a water-free lubricant with diamond suspension (<6 μm) was used on a polishing cloth (Struers). The analyzed chemical compositions, by inductively coupled plasma optical emission spectroscopy (Perkin Elmer 7300V), and T_g are given in **Table 1**.

The glass samples were isostatically compressed at a raised temperature using two nitrogen gas pressure chambers: one vertically positioned with an internal diameter of 6 cm for compression at 1 GPa and the other horizontally positioned with an internal diameter of 3 cm for compression at 2 GPa. A multizone and single zone cylindrical graphite furnace was used for compression at 1 and 2 GPa, respectively. To monitor the temperature during the experiments, PtRh6%–PtRh30% thermocouples were used. They were arranged in the furnaces and coupled with the input power control electronic systems. In both cases, the pressure was measured by manganin gauges. The pressures and temperatures were stabilized with an accuracy of 1 MPa and 0.1 K, respectively. Glass samples were placed in an alumina crucible and then heated in the furnaces inside the high-pressure reactors with a constant heating rate of 600 K/h

TABLE 1 | Analyzed chemical compositions, glass transition temperature (T_g), density (ρ), atomic packing density (C_g), and molar volume (V_m) of the as-prepared glasses.

Glass ID	Analyzed composition (mol%)				(T_g) (°C)	C_g (-)	ρ (gcm^{-3})	V_m(cm^{3}mol^{-1})
	Al_2O_3	CaO	P_2O_5	O/P ratio				
P60	0	40.4	59.6	2.84	472	0.518	2.521	42.5
P50	0	49.9	50.1	3.00	514	0.533	2.654	37.3
P46	0	53.9	46.1	3.08	525	0.540	2.718	35.2
Al5	5.0	40.2	54.8	3.00	534	0.533	2.614	40.3
Al10	10.0	30.1	59.9	3.00	558	0.534	2.585	43.4
Al15	14.8	20.0	65.2	2.99	602	0.540	2.583	46.0

The errors in T_g, ρ, and C_g, do not exceed ±2°C, ±0.002 g/cm^3, and ±0.001. respectively.

to the ambient pressure T_g value of each glass. The systems were kept at these conditions under high nitrogen pressure (1 or 2 GPa) for 30 min. Afterward, the furnace was cooled down to room temperature at a constant rate of 60 K/h, followed by decompression at a rate of 30 MPa/min.

Structural Characterization

Raman spectroscopy measurements were performed at room temperature to obtain information about the structure of glasses at short- and intermediate-range length scales. This was done using a Renishaw Invia micro-Raman spectrometer with 532 nm laser in the range from 200 to 1,600 cm^{-1}. The measurements were conducted on as-prepared and compressed samples. All Raman data were subjected to intensity normalization by dividing the intensities by the maximum intensity of each spectrum.

Solid state NMR spectra of ^{31}P were obtained using a commercial magic-angle spinning (MAS) NMR probe (Agilent) and spectrometer (Agilent DD2), in combination with an 11.7 T superconducting magnet. All the glass samples (powder) were loaded into 3.2 mm zirconia rotors and spun with compressed nitrogen at 20 kHz. The resonance frequency of ^{31}P at this external field strength was 202.30 MHz. Spectra were acquired with a 1.2 μs pulse width, corresponding to a π/6 tip angle, using a delay time of 240 s and as a composite of 60 to 220 free induction decays. Spectra were processed without any additional apodization and referenced to 85% H_3PO_4 in water (0 ppm). The fitting of ^{31}P MAS NMR data was made using DMFit (Massiot et al., 2002), using a minimum number of Gaussian lineshapes to represent Q^n species, and with full consideration of spinning sidebands when determining site populations.

^{27}Al MAS NMR spectra were collected using a commercial MAS NMR probe (Agilent) and spectrometer (DD2), with a narrow-bore 16.4 T superconducting magnet and thus a resonance frequency of 182.34 MHz. Powdered glass samples were contained in low Al background zirconia rotors and spun at 22 kHz. The data were acquired with very short (0.6 μs) pulse widths (π/12 tip angle), recycle delays of 4 s and with signal averaging of typically 1,000 scans. ^{27}Al MAS NMR data were processed without extra line broadening and referenced to aqueous aluminum nitrate at 0.0 ppm. Fitting of ^{27}Al MAS NMR spectra was conducted with DMFit using the "CzSimple" model to accurately represent the 2nd-order quadrupolar broadened lineshapes belonging to various Al coordination environments.

Property Characterization

Density (ρ) was determined using the Archimedes method by first weighing the sample in air and then weighing it when suspended in ethanol at room temperature. This was repeated a minimum of ten times for each sample. The standard deviation of the reported density values did not exceed ±0.002 g cm^{-3}. The molar volume (V_m) was calculated as the ratio between the molar mass of the glass and its density. Furthermore, we calculated the atomic packing density (C_g) of the glasses to evaluate the differences in the free volume of the glasses. C_g is the ratio between the minimum theoretical volume occupied by the ions (assumed to be spherical) and the corresponding molar volume of the glass. The value of C_g is calculated using effective ionic radii to calculate the minimum theoretical volume occupied by the ions (Shannon, 1976), assuming 6-fold coordination for Ca, 2-fold coordination for O, 4-fold coordination for P, and coordination number for Al as obtained from the NMR results.

A Vickers micro-indenter (Duramin 5, Struers) was used to determine hardness (H_V). The measurements were performed in air at room temperature with a relative humidity of 50 ± 5%. At least 30 indents were performed at loads of 0.05 and 0.2 kgf for CaO-P_2O_5 and 0.05 and 0.1 kgf for CaO-Al_2O_3-P_2O_5 glasses with a dwell time of 15 s. H_V was calculated from the size of the imprint at respective load.

Glass chemical durability in an aqueous solution was measured for as-made annealed glasses and compressed glasses. Samples with dimensions of about 10 × 10 × 3 mm^3 were immersed into 200 ml deionized H_2O at 40 °C for different time durations up to 428 h. The water was not stirred and the samples were suspended by Teflon line in the solution. The weight loss of samples was regularly measured for different time intervals.

RESULTS AND DISCUSSION

^{31}P and ^{27}Al MAS NMR Spectroscopy: As-Made Glasses

Figure 1 shows the ^{31}P MAS NMR spectra of both as-made and compressed glasses. The center band intensities are isotropic resonances that can be assigned to Q^3, Q^2, and Q^1 units. We use the standard Q^n nomenclature for phosphorus speciation, in which the exponent (n) indicates the number of bridging oxygen (BO) per phosphorous atom. The experimental spectra were simulated using Gaussian line shapes for each Q^n site. The

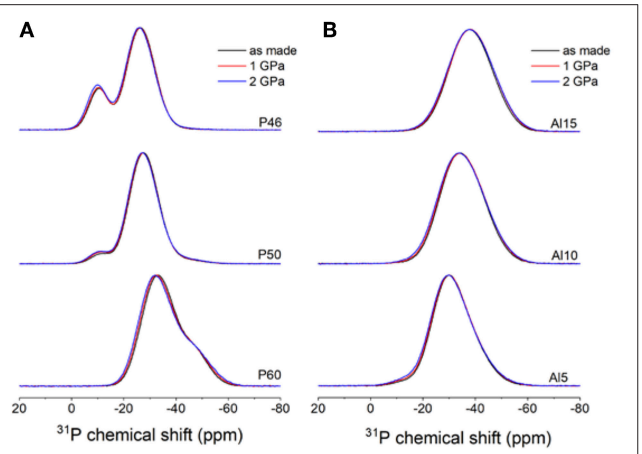

FIGURE 1 | ^{31}P MAS NMR spectra of the as-prepared glasses (black) and glasses hot compressed at 1 GPa (red) and 2 GPa (blue): **(A)** $CaO\text{-}P_2O_5$; **(B)** $CaO\text{-}Al_2O_3\text{-}P_2O_5$.

relative total area of each approximated isotropic peak and its associated sidebands was used as a measure of the respective site concentration. **Table 2** lists the isotropic chemical shifts (δ_{CS}) and the site concentrations determined for the phosphorous species in the present glasses.

First, we considered the as-made binary $CaO\text{-}P_2O_5$ glasses (**Figure 1A**). The ^{31}P spectrum of the ultraphosphate composition (P60, see **Table 1**) is dominated by isotropic peaks near −33 and −46 ppm, representing the Q^2 and Q^3 units, respectively (Brow, 2000). As expected, the spectrum of the metaphosphate composition (P50) is dominated by the Q^2 peak, but also contains small peaks for Q^1 and Q^3 tetrahedra. The relative peak areas for the different P polymerizations vary systematically with composition, i.e., with increasing CaO modifier content, the Q^3 peak decreases in intensity while that of Q^1 increases (**Table 2**). The observed P speciation is thus generally consistent with previous ^{31}P NMR results for Na- and Ca-phosphate glasses (Kirkpatrick and Brow, 1995; Brow, 1996). However, Na- and Ca-metaphosphate glasses exhibit different Q^n distribution, as the Na-metaphosphate glass contains predominantly Q^2 units, whereas the Ca-metaphosphate glass also features small but noticeable amounts of Q^1 and Q^3 units. The latter is due to the disproportionation reaction, i.e., $2Q^n \rightarrow Q^{n-1} + Q^{n+1}$, which is shifted to the right with increasing modifier field strength (charge-to-size ratio) (Fletcher et al., 1993). Furthermore, the chemical shift of the Q^2 peak shifts toward higher ppm values with increasing CaO content (**Table 2**). The change in the ^{31}P chemical shift with increasing CaO content in our glasses parallels the trend observed previously with increasing Na_2O content in $Na_2O\text{-}P_2O_5$ glasses (Kirkpatrick and Brow, 1995).

Next, we considered the as-made ternary $CaO\text{-}Al_2O_3\text{-}P_2O_5$ glasses (**Figure 1B**). The ^{31}P MAS NMR spectra contained several overlapping resonances that shows a progressive shift toward more negative ppm and a broadening with the increasing concentration of Al_2O_3. The observed results are similar to those observed in other alkali-alumino-metaphosphate glasses and have been attributed to the increasing formation of P-O-Al linkages in comparison to that of P-O-Ca (Schneider et al., 2003). Previous studies have reported similar shift in the positions of ^{31}P NMR peaks in alumino-metaphosphate glasses upon Al_2O_3 addition and have been correlated to general strengthening, or shortening, of the average P–O bonds related with the different metal polyhedra (Smith et al., 2014). Furthermore, it has been shown that the ^{31}P peak for a Q^2 unit connected to an alkali or alkaline earth ion will occur at a more positive chemical shift than the ^{31}P peak for a Q^2 unit connected to aluminum (Brow et al., 1993). Similar to the binary P50 composition, the ternary $CaO\text{-}Al_2O_3\text{-}P_2O_5$ metaphosphate glasses also feature small but non-negligible amounts of Q^3 and Q^1 units. The presence of Q^1 and concomitant Q^3 can also be explained by the disproportionation reaction. Furthermore, the deconvolution of the ternary glass spectra also indicates the presence of two distinct Q^2 units with resonances around −28 and −36 ppm, respectively. The former signal is attributed to Q^2 (0Al) units (where xAl represents the number of Al atoms as next nearest neighbor), while the latter is due to Q^2 (1Al) units as the formation of P-O-Al linkage leads to a shift of the ^{31}P resonance toward more negative ppm (i.e., shielded) by ∼7 to 8 ppm (Fletcher et al., 1993), consistent with the ∼8 ppm shift difference required to adequately fit the spectra (**Figure 2**).

Figure 3A shows the ^{27}Al MAS NMR spectra for the $CaO\text{-}Al_2O_3\text{-}P_2O_5$ glasses, with the site populations listed in **Table 3**. All three compositions yielded spectra with three peaks around 36, 6, and −17 ppm, which can be unambiguously assigned to Al^{IV}, Al^{V}, and Al^{VI} structural units, respectively (MacKenzie, 2002). The spectra show a decrease in the fraction of Al^{VI} species with increasing Al_2O_3 content, with Al^{VI} as the predominant species for all the compositions (**Figure 3B**). The results agree with previous investigations on aluminophosphate glasses, where Al predominantly exists in octahedral coordination within the metaphosphate (O/P ≈ 3) regime (Brow et al., 1990, 1993; Brow, 1993; Schneider et al., 2003). From the peak areas, the average coordination number (CN) of Al was calculated for the investigated glasses. The results are plotted in the inset of **Figure 3B**, showing a reduction of Al CN from 5.45 to approximately 5.28 with increasing Al_2O_3/CaO ratio. We also note that the present ^{27}Al NMR peak assignment is similar to that reported for Ca-aluminophosphate glasses with all Al bonded to P as next nearest neighbor (NNN) (Brow et al., 1990). On the other hand, the present glasses feature more shielded peaks relative to the ^{27}Al chemical shifts reported for aluminoborate and aluminosilicate glass (Bista et al., 2015). This shift upon introduction of phosphorus is likely due to the difference in electronegativity between phosphorus, silicon, and boron, which increases the shielding of the Al nucleus, resulting in a shift in these resonances by up to −25 ppm (MacKenzie, 2002).

^{31}P and ^{27}Al MAS NMR Spectroscopy: Densified Glasses

Structural changes in the P speciation upon hot compression have been found to be highly composition dependent, that

TABLE 2 | Phosphorus speciation obtained by deconvolution of ^{31}P MAS NMR spectra.

Glass ID	Q^1		Q^2		Q^3		*O/P ratio*
	Int (%)	δ_{CS} *(ppm)*	*Int (%)*	δ_{CS} *(ppm)*	*Int (%)*	δ_{CS} *(ppm)*	
P60	…	…	78.6	−32.9	21.4	−46.5	2.89
P60 (1 GPa)	…	…	74.6	−32.1	25.4	−45.9	2.87
P60 (2 GPa)	…	…	69.7	−31.5	30.3	−45.3	2.85
P50	4.1	−10.5	89.5	−27.7	6.4	−42.0	2.99
P50 (1 GPa)	4.5	−10.3	88.6	−27.4	6.9	−41.0	2.99
P50 (2 GPa)	4.9	−10.0	88.4	−27.2	6.8	−41.0	2.99
P46	18.3	−10.2	79.6	−26.5	2.1	−41.2	3.08
P46 (1 GPa)	18.5	−9.9	79.4	26.3	2.2	−41.2	3.08
P46 (2 GPa)	19.5	−9.7	78.4	−26.1	2.1	−41.2	3.09
Al5	1.6	−13.2	67.4	−28.9	5.0	−45.0	2.99
			25.9	−37.8			
Al5 (1 GPa)	2.4	−13.2	65.5	−28.7	7.0	−45.0	2.97
			25.0	−37.7			
Al5 (2 GPa)	3.1	−12.8	67.1	−28.6	5.3	−47.0	2.99
			24.5	−38.4			
Al10	1.2	−15.9	42.7	−30.0	14.2	−45.0	2.94
			41.9	−37.9			
Al10 (1 GPa)	1.4	−15.9	42.2	−29.7	16.9	−45.0	2.93
			39.5	−37.7			
Al10 (2 GPa)	1.6	−15.9	43.6	−29.5	18.6	−45.0	2.92
			36.1	−37.5			
Al15	0.2	−15.9	25.9	−32.6	19.7	−46.0	2.90
			54.1	−38.6			
Al15 (1 GPa)	0.3	−15.9	27.5	−32.2	25.9	−46.0	2.87
			46.3	−38.5			
Al15 (2 GPa)	0.4	−15.9	31.9	−31.9	28.5	−46.0	2.86
			39.2	−38.5			

Uncertainties in the Q^n populations and chemical shift (δ_{CS}) are ± 1% and ±1 ppm, respectively. (O/P ratio = (2.5[Q^3] + 3*[Q^2] + 3.5*[Q^1] + 4*[Q^0])/100, in which [Q^n] is the Int% by NMR deconvolution.)*

is, the phosphorus network undergoes depolymerization upon hot compression of (72-x)SiO_2-20B_2O_3-xP_2O_5-8Al_2O_3 glasses (Kapoor et al., 2017a), while in case of binary zinc phosphate and another SiO_2-B_2O_3-P_2O_5-Al_2O_3 glass, only minimal changes in the P network were observed (Kapoor et al., 2017b, 2018). In the present investigation, hot compression of the glasses results in insignificant changes in the ^{31}P chemical shifts and relative areas of the peaks corresponding to different Q^n phosphorous units (**Table 2**). Significant changes are only observed in the ultraphosphate glass (P60), where the pressure treatment at 2 GPa induces a 9% increase in the relative amount of Q^3 units at the expense of Q^2 units (**Table 2**). No significant changes are observed in the glasses with higher O/P ratio. The minimal changes in the P speciation upon compression agrees with the previous studies on pressure quenched ν-P_2O_5 by Brazhkin et al. using ^{31}P MAS NMR and X-ray diffraction studies (Brazhkin et al., 2011). Considering further the CaO-Al_2O_3-P_2O_5 glasses, compression induces even more subtle changes in the ^{31}P NMR spectra (**Figure 1**). **Table 2** shows that the quantitative changes upon compression are well within the uncertainty values expected in deconvolution.

As a glass is compressed, the ionic environments can change in different ways, including a coordination number increase, a change in bond distances, angles, and in the types and amounts of linkages present (e.g., P-O-Al, P-O-P). In the case of Al, the most obvious structural change is an increase in coordination number, as observed in various oxide glasses (Allwardt et al., 2004; Kapoor et al., 2017c). The comparative abundance of each aluminum species is proportional to the area under its peak and the fitted values are given in **Table 3**. The peak areas corresponding to Al^V and Al^{VI} are greater for the samples recovered from hot compression (1 and 2 GPa) in comparison to those at ambient pressure. The quantitative change in Al coordination per unit change in pressure increases with increasing [Al_2O_3]/[CaO] ratio (**Figure 3C**). It is noteworthy that compression at 1 GPa results in a relatively large change in the degree of polymerization of Al in comparison to that at 2 GPa, i.e., after increasing the pressure further to 2 GPa, relatively small changes are observed in the glass reticulation. The ^{27}Al NMR spectra (**Figure 3A**)

show a slight increase in the frequency of the Al^{VI} resonance and a decrease for Al^{IV} and Al^{V} peaks, upon compression. Analogous to aluminosilicates glasses, the high frequency shift in ^{27}Al spectra may be related to the decrease in bond angles, while the low frequency shift could be due to the development of links between high-coordinated Al sites (Kelsey et al., 2009). Further, in the case of phosphate and aluminophosphate glasses, network forming cations Al and P can both respond to pressure changes by changing their local environment. However, the observed structural changes for Al upon compression are more pronounced than those for P, suggesting that the threshold energy

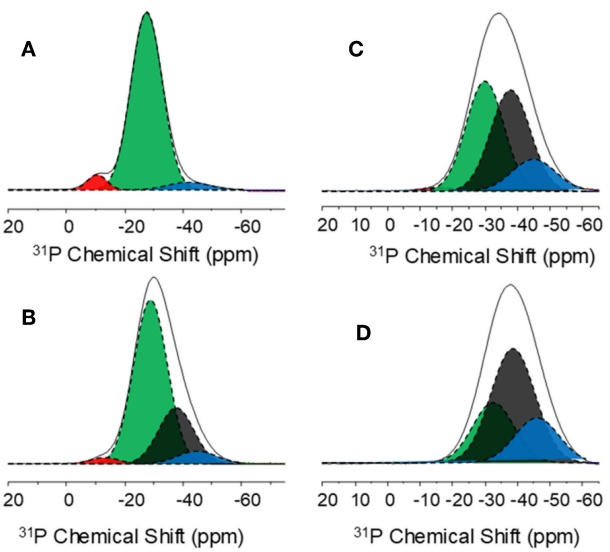

FIGURE 2 | Deconvolution of ^{31}P MAS NMR spectra for **(A)** P50, **(B)** Al5, **(C)** Al10, and **(D)** Al15 glasses. Q^1, Q^2 and Q^3 peaks are indicated by red, green, and blue curves. The black Gaussian peak represents the $Q^{2,1}$ peak formed in Al-containing glasses.

TABLE 3 | Aluminum speciation and associated NMR parameters obtained by deconvolution of ^{27}Al MAS NMR spectra.

Glass ID	Al^{IV}		Al^{V}		Al^{VI}	
	Int (%)	δ_{CS} (ppm)	Int (%)	δ_{CS} (ppm)	Int (%)	δ_{CS} (ppm)
Al5	8.6	35.3	38.2	5.9	53.2	−18.0
Al5 (1 GPa)	4.8	35.0	31.9	5.5	63.2	−18.2
Al5 (2 GPa)	3.5	34.8	27.9	4.9	68.8	−18.2
Al10	12.6	35.6	41.0	6.3	46.4	−17.3
Al10 (1 GPa	6.9	35.5	34.9	5.9	58.2	−17.5
Al10 (2 GPa)	4.3	35.3	30.5	5.7	65.2	−17.4
Al15	15.2	36.3	41.6	6.9	43.3	−16.4
Al15 (1 GPa	7.5	35.9	35.3	6.4	57.2	−16.6
Al15 (2 GPa)	4.4	35.6	30.3	6.1	65.3	−16.6

The uncertainties in intensity (Int) and isotropic chemical shift (δ_{CS}) are estimated to be 2%, and 1 ppm, respectively.

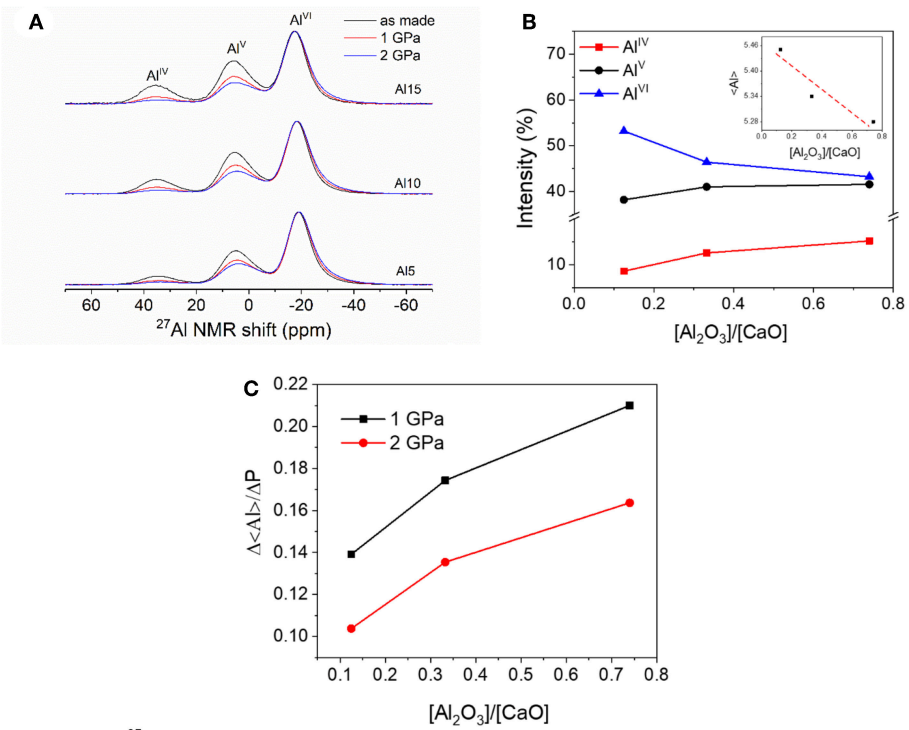

FIGURE 3 | (A) ^{27}Al MAS NMR spectra of as-prepared CaO-Al_2O_3-P_2O_5 glasses (black) and those hot compressed at 1 GPa (red) and 2 GPa (blue). **(B)** Intensities of each central ^{27}Al NMR line as a function of the glass composition. Inset: mean coordination number for Al calculated from the NMR intensities. **(C)** Composition dependence of the change in the mean Al coordination (<Al>) per unit change in pressure.

required for the structural changes upon compression in case of aluminophosphate glasses is higher for P compared to Al.

Raman Spectroscopy

We next considered the Raman spectra of the as-prepared and compressed $CaO\text{-}P_2O_5$ (**Figure 4A**) and $CaO\text{-}Al_2O_3\text{-}P_2O_5$ (**Figure 4B**) glasses between 200 and 1,500 cm^{-1}. In general, the Raman spectra are characterized by strong features in the mid-frequency (600–850 cm^{-1}) and high-frequency regions (950–1,400 cm^{-1}), with additional minor features in the low-frequency region (200–400 cm^{-1}).

The $CaO\text{-}P_2O_5$ glasses feature a broad band around 340 cm^{-1}, which has been attributed to vibrations of phosphate polyhedra (Meyer, 1998). In the mid-frequency region, the bands in the region from 650 to 850 cm^{-1} are attributed to stretching modes associated with BOs, linking two neighboring tetrahedra $(POP)_{sym}$ (Meyer, 1998). For the P60 glass, the band is centered around 666 cm^{-1} and assigned to the stretching modes associated with ν_s(P–O–P) (Meyer, 1998). The location of this band shifts toward higher frequency with increasing CaO content, as it is observed around 694 cm^{-1} for P50 and P46 glasses. As discussed above, the structure of the P60 glass primarily consists of Q^2 and Q^3 units, where Q^3 is primarily bonded to Q^2 units (Q^2-Q^3). That is, a cross-linked network dominated by Q^2-Q^3 and Q^2-Q^2 interactions, where Q^2-Q^2 chains dominate the glass network (**Table 2**). These chains are broken upon CaO addition, thus forming chain terminating Q^1 units attributed to the collective effect of modifier addition and disproportionation reactions (Fletcher et al., 1993). Therefore, the shifting of the Raman band (666 cm^{-1}) to higher frequency with increasing CaO content could be ascribed to the decrease in the average phosphate chain length when the NBO content increases (Brow, 2000).

The high-frequency region consists of bands associated with the symmetric and asymmetric stretching modes of NBOs on different P tetrahedra, along with the band due to stretching of $(P{=}O)_{sym}$ (Meyer, 1998). The P60 composition features two prominent bands in this region (**Figure 4A**). The band around 1174 cm^{-1} corresponds to $\nu(PO_2)_{sym}$, while that near 1,306 cm^{-1} is attributed to $(P{=}O)_{sym}$, and is consistent with the Q^3 environment identified in the ^{31}P MAS NMR spectra. The width of the $\nu(PO_2)_{sym}$ band is generally smaller than that of $(P{=}O)_{sym}$, indicating that the Q^3 tetrahedra exhibit wider bond angle distributions than the Q^2 tetrahedra. The relative intensity of the 1,174 cm^{-1} band increases upon CaO addition due to the increase in the number of NBOs. We also note that the addition of CaO results in disappearance of the band associated with $(P{=}O)_{sym}$, also similar to the reduction of Q^3 in the ^{31}P NMR data. This agrees with the findings of Hudgens et al. (1998), suggesting that modifier addition decreases the symmetry of $(P{=}O)_{sym}$ bond, resulting in an asymmetric bond which becomes indistinguishable from the $(PO_2)_{sym}$ mode of Q^2 tetrahedra. An additional weaker band at 1,018 cm^{-1} was observed in the P46 glass, which could be assigned to the symmetric stretching vibrations of the pyrophosphate Q^1 end-group units $\nu_s(PO_3^{2-})$ (Meyer, 1998).

Densification of the binary glasses at 1 and 2 GPa leads to changes in the Raman peak positions, with the most prominent changes in the mid-frequency region (**Figures 5A,B**) and minimal changes in the high-frequency region (**Figures 5A,B**). The changes in the mid-frequency region could be attributed to changes in the P-O-P bond angles. In the P60 and P50 glasses, the band corresponding to P-O-P shifts toward higher frequency upon hot compression, indicating a decrease in the P-O-P average bond angle (**Figure 5A**). This shift toward higher Raman band frequency upon compression has been observed for a wide range of vibrational modes and compositions, including silicates (Hemley et al., 1986; Mysen and Frantz, 1994), germanates (Le Parc et al., 2009), solid argon (Crawford et al., 1978; Watson and Daniels, 1988), and carbon-based solids (Boppart et al., 1985; Sandler et al., 2003). However, for the P46 glass, we observe a shift toward lower frequency upon compression (**Figure 5B**), which is analogous to the change observed in our recent high-pressure study on zinc phosphate glass with composition between meta- and pyro-phosphate regions (Kapoor et al., 2017b). Different responses to pressure exhibited by the high-P and low-P glasses here are indeed similar to how the P speciation as determined by ^{31}P MAS NMR is different for the P60 and P46 glasses (**Figure 1A**), confirming that the O/P ratio appears to dictate the network's response to compression.

The Raman spectra for the binary and ternary glasses are similar (**Figure 4**). This suggests that metaphosphate chains also dominate the structure in calcium aluminophosphate glasses, as indicated by the total Q^2 population determined for these glasses. With increasing aluminum content in these glasses, we observe a systematic change in the relative intensity and position of the bands, although the general pattern of the spectra remains similar (**Figure 5B**). This is consistent with spectroscopic studies of mixed alkali and alkaline earth metaphosphate glasses that reveal similar systematic changes in the nature of the phosphate network with modifier substitution (Rouse et al., 1978; Sato et al., 1992). Furthermore, addition of Al results in a shift of the high-frequency region band corresponding to P-NBO vibration from 1,188 to 1,220 cm^{-1}. The systematic changes in the Raman peaks agree with the peak shift observed in the ^{31}P NMR spectra where both spectral trends show a general strengthening, or shortening, of the average P–O bonds related with the different metal polyhedra (Smith et al., 2014). A previous study by Schneider et al. (2005) has correlated the positive shift in frequency with Al_2O_3 addition to two predominant factors: firstly to the increased interaction among the NBOs with the Al cation and secondly to the increased fraction of Al-O bonds, which exhibit larger bond strength than Ca-O. In addition, changes in the relative intensities of P-BO and P-NBO Raman peaks for metaphosphate glasses indicate that higher field strength cations produce stronger P–NBO bonds (Nelson and Exarhos, 1979). In contrast to the binary phosphate glasses, there are no systematic shifts in bands in the mid- and high-frequency regions upon compression of the ternary systems (**Figure 5B**).

Density, Molar Volume, Atomic Packing Density, and Plastic Compressibility

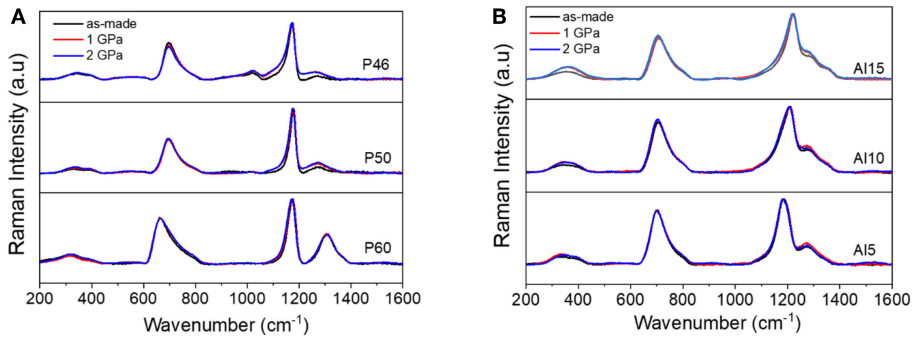

FIGURE 4 | Raman spectra of the as-prepared and compressed glasses: **(A)** $CaO\text{-}P_2O_5$ and **(B)** $CaO\text{-}Al_2O_3\text{-}P_2O_5$.

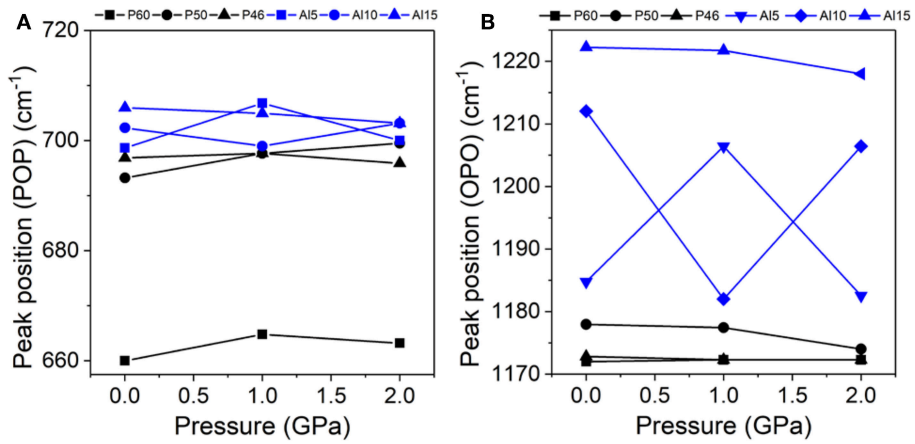

FIGURE 5 | Pressure dependence of the positions of the Raman bands corresponding to **(A)** P–O–P vibrations and **(B)** O–P–O vibrations for the binary and ternary phosphate glasses.

Figure 6 and **Table 1** show the variation of density (ρ), molar volume (V_m), and atomic packing density (C_g) with composition and pressure for the two series of glasses. For the as-prepared binary glasses, substitution of P_2O_5 by CaO results in an increase in density and a decrease in the molar volume (**Figure 6A**) accompanied by an increase in C_g of the glasses (**Table 1**). For the ternary glasses, addition of Al_2O_3 results in lower density in part due to the simultaneous reduction of CaO content (**Figure 6B**) and a concomitant increase in C_g (**Table 1**).

Following hot compression of the samples, the density of all glasses increases due to network compaction, in agreement with results for other oxide glasses in a similar pressure/temperature regime (Kapoor et al., 2017c). However, the magnitude of the pressure-induced change in density varies with composition, which can be evaluated by calculating the plastic compressibility (β), which is defined as the volume (V) change measured after decompression to ambient pressure, i.e., $-(1/V)(dV/dp)$ (Kapoor et al., 2017c). The plastic compressibility of binary phosphate decreases with the increase in CaO content, but it increases with increasing Al_2O_3/CaO ratio in the ternary glasses (**Figure 7**). We note that the plastic compressibility is negatively correlated to the C_g of the ambient condition glasses, suggesting that the free volume in the glasses accommodates the densification upon hot compression (inset of **Figure 7**) (Striepe et al., 2013). However, in the case of the aluminophosphate glasses, the volume densification is positively correlated to the C_g of the as-prepared glasses (inset of **Figure 7**) along with the change in mean alumina coordination number (**Figure 3C**). This apparent correlation could suggest that the Al CN change is an important densification mechanism for these ternary glasses.

Furthermore, and in agreement with previous studies, the β of the investigated glasses decreases with increasing pressure, i.e., a smaller observed increment in density when increasing the pressure from 1 to 2 GPa compared to that from ambient pressure to 1 GPa (**Figure 7**). The decrease in the plastic compressibility can be intuitively understood as initial compression first consumes the easiest available free volume and flexible structural units in the glass (Kapoor et al., 2017b). As discussed based on the Raman and NMR results above, the observed volume densification is mostly associated with changes in the inter-tetrahedral bond angles, and to the degree of polymerization of the glass network, as

well as changes in coordination number of Al in the ternary glasses (Kapoor et al., 2017c).

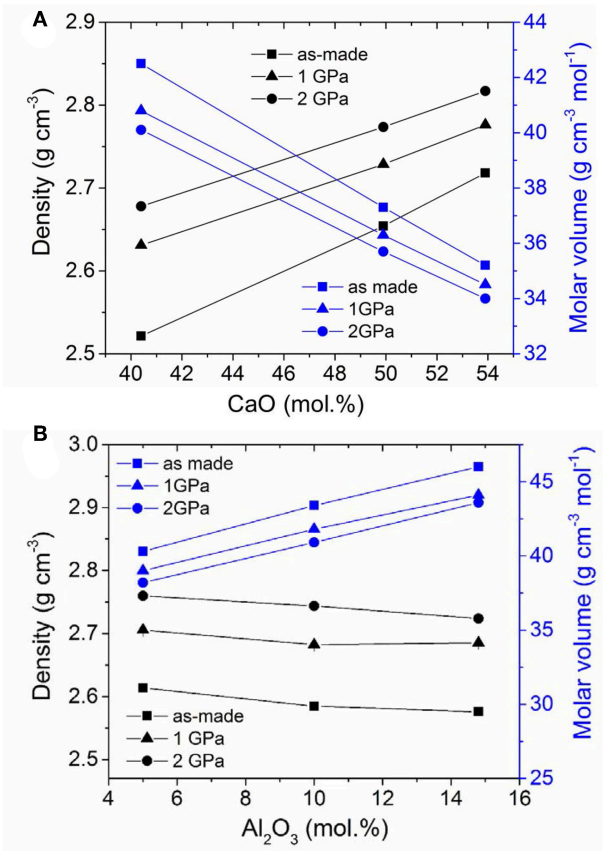

FIGURE 6 | Density and molar volume of as-prepared and hot compressed glasses as a function of the molar concentration of **(A)** CaO and **(B)** Al_2O_3 in $CaO\text{-}P_2O_5$ and $CaO\text{-}Al_2O_3\text{-}P_2O_5$ glasses, respectively. The errors associated with the density values are smaller than the size of the symbols.

Vickers Hardness

Indentation experiments on the $CaO\text{-}P_2O_5$ and $CaO\text{-}Al_2O_3\text{-}P_2O_5$ glasses provide insight into the resistance of glasses toward elastoplastic deformation, as quantified by Vickers hardness H_V (**Figure 8**). H_V of the calcium phosphate glasses increases with increasing CaO content (**Figure 8A**), indicating that the stacking of phosphate chains is more compact with an increase in the packing fraction of glasses (**Table 1**), as evident from the increase in molar volume and decrease of C_g with CaO addition. This space filling increases the number of bond constraints per volume, providing rigidity to the network, despite having a depolymerizing effect, and thus higher hardness for the high-CaO glasses. Previous studies indicate a similar increase in H_V of binary phosphate glasses with increasing CaO content (Rao and Shashikala, 2014). In the calcium aluminophosphate glasses, the addition of Al_2O_3 results in an increase in H_V (**Figure 8B**). This increase is attributed to the collective contribution from the increase in degree of network connectivity and average bond strength. The former is due to an increase in the Al_2O_3 concentration, which results in an increase in the average number of bond constraints per atom (Smedskjaer et al., 2010), while the latter is due to the higher field strength of the Al^{3+} cation. A similar trend is observed for T_g (**Table 1**), implying that both properties have similar structural origins, as also illustrated from the positive correlation between T_g and H_V (**Figure 9**) for a variety of different phosphate glasses.

Hot compression of the glasses results in an increase in H_V (**Figure 8**). This effect is qualitatively similar to previously investigated glass systems in the same pressure/temperature regimes (Kapoor et al., 2017b,c). However, consistent with the density results, we observe a larger increase in H_V from 0 to 1 GPa in comparison to that from 1 to 2 GPa, suggesting that the overall network densification is responsible for the increase in hardness. The volume densification facilitates a larger resistance to densification when subjected to sharp-contact loading at room temperature. It is worth noting that for the glasses compressed at 2 GPa, the H_V values remain similar despite the compositional differences.

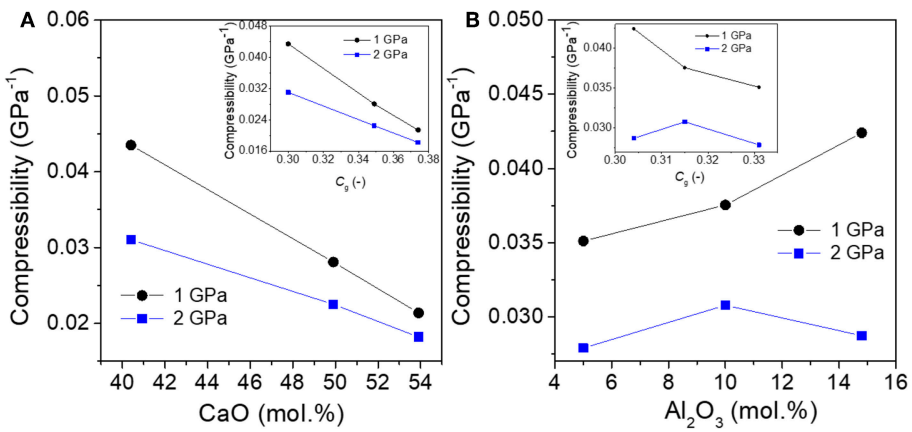

FIGURE 7 | Plastic compressibility (β) of compressed glasses as a function of the molar concentration and atomic packing density (C_g) (inset) of **(A)** CaO and **(B)** Al_2O_3 in $CaO\text{-}P_2O_5$ and $CaO\text{-}Al_2O_3\text{-}P_2O_5$ glasses, respectively.

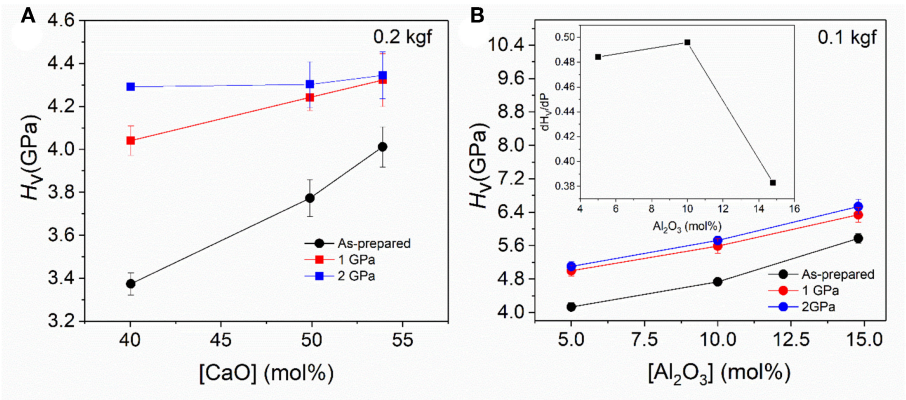

FIGURE 8 | Composition and pressure dependence of Vickers Hardness (H_V) of **(A)** CaO-P_2O_5 glasses and **(B)** CaO-Al_2O_3-P_2O_5 glasses. Inset in **(B)** shows dH_V/dP at 2 GPa, featuring similar trend as the plastic compressibility of the glasses at 2 GPa.

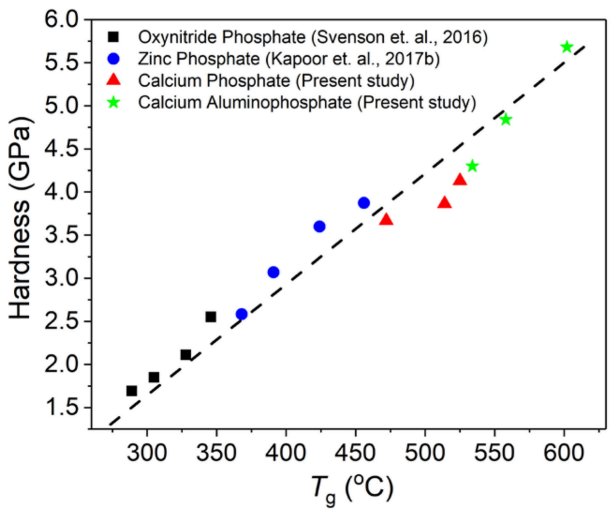

FIGURE 9 | Relationship between Vickers hardness (H_V) and T_g for various phosphate-based glasses (Svenson et al., 2016; Kapoor et al., 2017b). All the H_V values in the figure are obtained from tests conducted at 0.05 kgf load.

Chemical Durability

We investigated the chemical durability of selected as-made and compressed glasses (at 2 GPa) by measuring the weight loss in deionized water at 40°C (**Tables 4**, **5**). The weight loss is normalized by the initial surface area as a function of dissolution time. Aqueous corrosion of oxide glasses can generally occur through various processes, initially comprising hydration, ion exchange, and/or hydrolysis, depending on the glass composition and solution pH. Bunker et al. (1984) suggested that the dominating reaction in phosphate glass dissolution is the modifier–H^+ ion exchange reaction, dividing the dissolution process into two kinetic periods according to the profiles of dissolved amount (q) vs. time (t). That is, a decelerating dissolution period of $q \sim t^{1/2}$ and a uniform dissolution period of $q \sim t^1$. Furthermore, more recent studies

TABLE 4 | Mean weight loss (mg cm^{-2}) of CaO-P_2O_5 glasses after 24 h of immersion in deionized water at 40°C.

Glass ID	as-made	2 GPa
P60	0.98 ± 0.00	0.50 ± 0.05
P50	0.97 ± 0.11	0.79 ± 0.08
P46	0.77 ± 0.03	0.66 ± 0.03

propose that hydration and hydrolysis (breaking of P-O-P network bonds) play an interrelated role in glass dissolution, even proposing that hydrolysis reactions may dominate over hydration processes in metaphosphate glasses (Gao et al., 2004; Tošić et al., 2013). It is also possible that higher H^+ concentrations in acidic solutions may lead to elevated rates of hydration, thus accelerating the release rate of phosphate chains. On the other hand, in neutral–to–basic solutions (rich in H_2O or OH^-), where the degradation rate increases with pH, a hydrolysis-driven or alternate mechanism could be important, as H^+ is not readily available to hydrate non-bridging oxygens (NBOs) in the network (Tošić et al., 2013). However, some studies on binary Cu-phosphate glasses have reported that P-O-P bonds in linear phosphate chains are as resistant to hydrolysis as Si-O-Si bonds in neutral pH solutions, indicating that hydrolysis reactions may only be accelerated in acidic, but not in basic solutions.

Plots of weight loss in deionized water vs. time for the P50 glass are shown in **Figure 10**. The water-glass interaction gives rise to a general increase in weight loss within the time scale of the dissolution experiments. The chemical durability of the binary calcium phosphate glasses prepared at ambient conditions increases with increasing CaO content, as seen from a decrease in the weight loss from 0.97 to 0.77 gm cm^{-2} (**Table 4**). This increase in chemical durability has previously been attributed to the ability of Ca^{2+} to serve as ionic crosslinks between the NBOs of two different phosphate chains, thus increasing the chemical durability (Bunker et al., 1984). However, there is no further increase in chemical durability when the divalent

TABLE 5 | Mean weight loss (mg cm^{-2}) of $CaO\text{-}Al_2O_3\text{-}P_2O_5$ glasses after 428 h of immersion in deionized water at 40°C.

Glass ID	as-made	2 GPa
P50	14.61 ± 0.21	6.56 ± 0.68
Al5	0.45 ± 0.02	0.42 ± 0.07
Al10	0.13 ± 0.02	0.14 ± 0.03

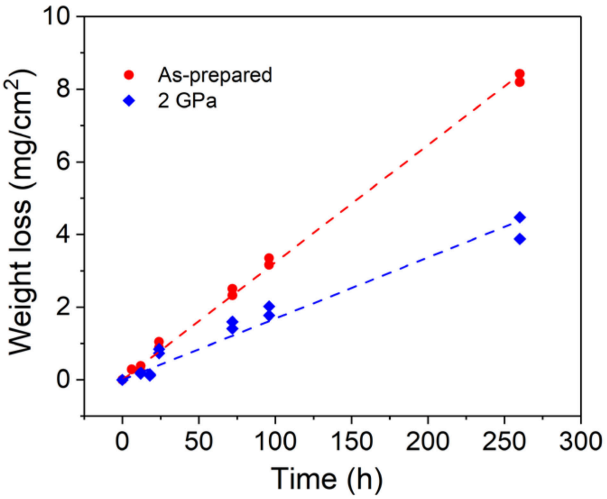

FIGURE 10 | Normalized weight loss (mg cm^{-2}) of the metaphosphate (P50) glass (as-prepared and compressed at 2 GPa) in deionized water as a function of dissolution time. The dashed lines represent linear fits to the data.

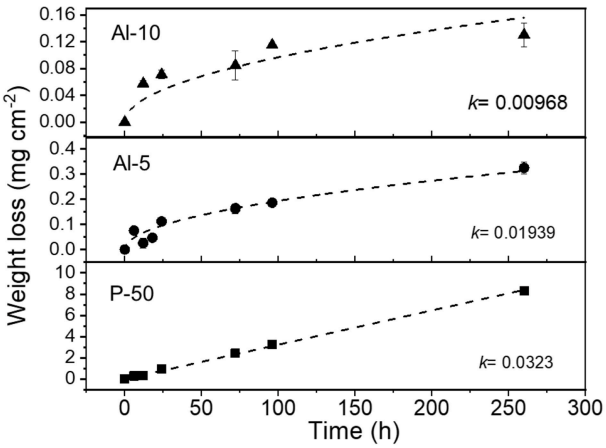

FIGURE 11 | Normalized weight loss (mg cm^{-2}) of the metaphosphate (P50) glass and $CaO\text{-}Al_2O_3\text{-}P_2O_5$ (Al5 and Al10) glass along with dissolution rate parameter (k) in deionized water as a function of time. The lines are drawn as guide for the eyes.

cation content reaches a certain point, because the polymer chains can only accommodate a limited number of chelate cross links (Bunker et al., 1984; Gao et al., 2004). Replacement of CaO by Al_2O_3 in calcium metaphosphate glasses (O/P = 3) improves the chemical durability by several orders of magnitude. While the binary phosphate glass experiments show a highly linear dependence of normalized weight loss (WL) on time ($WL = k \times t$), introduction of Al_2O_3 leads to half time dependence ($WL = k \times t^{1/2}$), as shown in **Figure 11**. After 428 h of dissolution, the metaphosphate glass (P50) exhibits ~14.6 g cm^{-2} of weight loss, while the Ca-Al-P glass with 10 mol% of Al_2O_3 has ~0.13 g cm^{-2} of weight loss (**Table 5**). Furthermore, the differences in WL vs. t curve shape as a function of Al_2O_3 content suggest a composition dependent shift in dissolution mechanism.

The effects of Al_2O_3 on the chemical durability and hardness of these calcium phosphate glasses are consistent with the widely reported structural role of Al_2O_3 in oxide glasses (Brow, 1993; Brow et al., 1993). Addition of Al_2O_3 strengthens the glass network by cross-linking phosphate chains, introducing relatively hydrolysis- and stress-resistant bonds into the phosphate network (i.e., Al-O-P and Al-O-Al), along with increasing the overall degree of network connectivity through formation of Al^{V} and Al^{VI} units. The resulting increase in structural polymerization degree is consistent with the increase in H_V, T_g, and chemical durability. Similar changes in chemical durability are also observed in silicate glasses, where the presence of Al_2O_3 impedes the molecular water from entering the glass network through the limited ability of H^+/H_3O^+ to ion-exchange for modifier ions and charge-compensate $[AlO_4]^-$ tetrahedra (Hamilton and Pantano, 1997). This makes it difficult to mobilize Na ions bonded to Al tetrahedra, resulting in enhanced chemical durability (Hamilton and Pantano, 1997).

Tables 4, **5** show the effect of densification on the chemical durability of the binary and ternary phosphate glasses. In general, we observe an enhancement of the corrosion resistance following permanent densification. This is likely due to an increase of C_g, because of the decline in the average bond angle and void volume, and a higher network connectivity. Previous studies on binary sodium silicate and borate glasses reported an increase in the chemical durability upon compression up to 5 GPa at T_g due to a decrease of the Na^+ release rate (Zhang et al., 1991a,b), which was in turn attributed to the decrease in void volume available for water migration into reactive sites (Mascaraque et al., 2017).

CONCLUSIONS

We investigated the influence of high-temperature densification on the structure, mechanical properties (Vicker's hardness), and chemical durability (weight loss in water) of binary $CaO\text{-}P_2O_5$ and ternary $CaO\text{-}Al_2O_3\text{-}P_2O_5$ glasses. We found that the changes in P speciation in P_2O_5-based glasses upon hot compression are generally small and highly composition dependent. In the $CaO\text{-}Al_2O_3\text{-}P_2O_5$ glasses, the compression induced an increase in the Al coordination number, the extent of which increases with an increasing $[Al_2O_3]/[CaO]$ ratio. The extent of volume densification upon hot compression also varies with composition, as the plastic compressibility of binary phosphate

decreases with the increase in CaO content, but increases with an increasing Al_2O_3/CaO ratio in ternary glasses. Furthermore, in the case of the aluminophosphate glasses, the observed extent of volume densification was positively correlated to the C_g and the change in the mean Al coordination number. In general, and as previously found for other oxide glasses, we observed an enhancement of hardness and corrosion resistance following permanent densification. This is likely due to an increased atomic packing density, because of the decrease in the average bond angle and free volume, and the increased network connectivity.

AUTHOR CONTRIBUTIONS

All authors listed have made a substantial, direct and intellectual contribution to the work, and approved it for publication.

FUNDING

This work was supported by the Independent Research Fund Denmark under Sapere Aude: DFF-Starting Grant (1335-00051A). MB acknowledges support from the National Science Foundation under Grants No. 1562066, 1762292, and 1826420.

REFERENCES

Aitken, B. G. (2008). *High Strain Point Glasses*. US20050142364A1.

Allwardt, J. R., Schmidt, B. C., and Stebbins, J. F. (2004). Structural mechanisms of compression and decompression in high-pressure $K_2Si_4O_9$ glasses: an investigation utilizing Raman and NMR spectroscopy of glasses and crystalline materials. *Chem. Geol.* 213, 137–151. doi: 10.1016/j.chemgeo.2004.08.038

Bista, S., Stebbins, J. F., Hankins, W. B., and Sisson, T. W. (2015). Aluminosilicate melts and glasses at 1 to 3 GPa: temperature and pressure effects on recovered structural and density changes. *Am. Mineral.* 100, 2298–2307. doi: 10.2138/am-2015-5258

Boppart, H., Straaten, J. V., and Silvera, I. F. (1985). Raman spectra of diamond at high pressures. *Phys. Rev. B*. 32, 1423–1425.h doi: 10.1103/PhysRevB.32.1423

Brazhkin, V. V., Akola, J., Katayama, Y., Kohara, S., Kondrin, M. V., Lyapin, A. G., et al. (2011). Densified low-hygroscopic form of P_2O_5 glass. *J. Mater. Chem.* 21, 10442–10447. doi: 10.1039/c1jm10889a

Brazhkin, V. V., Katayama, Y., Lyapin, A. G., and Saitoh, H. (2014). P-T phase diagram and structural transformations of molten P_2O_5 under pressure. *Phys. Rev. B* 89:104203. doi: 10.1103/PhysRevB.89.104203

Brow, R. K. (1993). Nature of alumina in phosphate glass: I, properties of sodium aluminophosphate glass. *J. Am. Cer. Soc.* 76, 913–918. doi: 10.1111/j.1151-2916.1993.tb05315.x

Brow, R. K. (1996). An XPS study of oxygen bonding in zinc phosphate and zinc borophosphate glasses. *J. Non Cryst Solids* 194, 267–273. doi: 10.1016/0022-3093(95)00500-5

Brow, R. K. (2000). The structure of simple phosphate glasses. *J. Non Cryst Solids* 263, 1–28. doi: 10.1016/S0022-3093(99)00620-1

Brow, R. K., Kirkpatrick, R. J., and Turner, G. L. (1990). Local structure of $xAl_2O_3 \cdot (1-x)NaPO_3$ glasses: an NMR and XPS study. *J. Am. Cer. Soc.* 73, 2293–2300. doi: 10.1111/j.1151-2916.1990.tb07591.x

Brow, R. K., Kirkpatrick, R. J., and Turner, G. L. (1993). Nature of alumina in phosphate glass: II, structure of sodium alurninophosphate glass. *J. Am. Ceram. Soc.* 76, 919–928. doi: 10.1111/j.1151-2916.1993.tb05316.x

Bunker, B. C., Arnold, G. W., and and Wilder, J. A. (1984). Phosphate-glass dissolution in aqueous-solutions. *J. Non Cryst. Solids* 64, 291–316. doi: 10.1016/0022-3093(84)90184-4

Chan, J. C. C., Bertmer, M., and Eckert, H. (1998). Double-quantum cross-polarization between half-integer quadrupolar spin systems: $^{11}B \leftrightarrow ^{23}Na$ and $^{11}B \leftrightarrow ^{27}Al$. *Chem. Phys. Let.* 292, 154–160. doi: 10.1016/S0009-2614(98)00660-5

Chan, J. C. C., Bertmer, M., and Eckert, H. (1999). Site connectivities in amorphous materials studied by double-resonance NMR of quadrupolar nuclei: high-resolution ^{11}B - ^{27}Al spectroscopy of aluminoborate glasses. *J. Am. Chem. Soc.* 121, 5238–5248. doi: 10.1021/ja983385i

Crawford, R. K., Bruns, D. G., Gallagher, D. A., and Klein, M. V. (1978). Raman scattering from condensed argon. *Phys. Rev. B* 17, 4871–4883. doi: 10.1103/PhysRevB.17.4871

Ellison, A., and Cornejo, I. A. (2010). Glass substrates for liquid crystal displays. *Int. J. Appl. Glass Sci.* 1, 87–103. doi: 10.1111/j.2041-1294.2010.00009.x

Ellison, A. J., Mauro, J. C., and Venkataraman, N. (2014). *Alkali-Free Phosphoborosilicate Glass*. WO2014182753A1.

Fletcher, J. P., Kirkpatrick, R. J., Howell, D., and Risbud, S. H. (1993). ^{31}P Magic-angle spinning nuclear magnetic resonance spectroscopy of calcium phosphate glasses. *J. Chem. Soc. Faraday Trans.* 89, 3297–3299. doi: 10.1039/ft9938903297

Gan, H., Hess, P. C., and Kirkpatrick, R. J. (1994). Phosphorus and boron speciation in K_2O-B_2O_3-SiO_2-P_2O_5 glasses. *Geochim. Cosmochim. Acta*, 58, 4633–4647. doi: 10.1016/0016-7037(94)90196-1

Gao, H. S., Tan, T. N., and Wang, D. H. (2004). Dissolution mechanism and release kinetics of phosphate controlled release glasses in aqueous medium. *J. Cont. Rel.* 96, 29–36. doi: 10.1016/j.jconrel.2003.12.031

Gauvin, M., Dassenoy, F., Minfray, C., Martin, J. M., Montagnac, G., and Reynard, B. (2007). Zinc phosphate chain length study under high hydrostatic pressure by Raman spectroscopy. *J. Appl Phys.* 101:063505. doi: 10.1063/1.2710431

Gauvin, M., Minfray, C., Belin, M., Aquilanti, G., Martin, J. M., and Dassenoy, F. (2013). Pressure-induced amorphization of zinc orthophosphate—Insight in the zinc coordination by XAS. *Tribology Int.* 67, 222–228. doi: 10.1016/j.triboint.2013.07.011

Gross, T. M. (2012). Deformation and cracking behavior of glasses indented with diamond tips of various sharpness. *J. Non Cryst. Solids* 358, 3445–3452. doi: 10.1016/j.jnoncrysol.2012.01.052

Gross, T. M., and Guo, X. (2015). *Damage Resistant Glass With High Coefficient of Thermal Expansion*. US9969644B2.

Hamilton, J. P., and Pantano, C. G. (1997). Effects of glass structure on the corrosion behavior of sodium-aluminosilicate glasses. *J. Non-Cryst. Solids* 222, 167–174. doi: 10.1016/S0022-3093(97)90110-1

Hemley, R. J., Mao, H. K., Bell, P. M., and Mysen, B. O. (1986). Raman spectroscopy of SiO_2 glass at high pressure. *Phys. Rev.Lett.* 57, 747–750. doi: 10.1103/PhysRevLett.57.747

Hirao, K., Yoshimoto, M., Soga, N., and Tanaka, K. (1991). Densification of magnesium and calcium metaphosphate glasses. *J. Non-Cryst. Solids* 130, 78–84. doi: 10.1016/0022-3093(91)90158-3

Huang, L., and Kieffer, J. (2004). Amorphous-amorphous transitions in silica glass. *I.* Reversible transitions and thermomechanical anomalies. *Phys. Rev. B* 69:224203. doi: 10.1103/PhysRevB.69.224203

Hudgens, J. J., Brow, R. K., Tallant, D. R., and Martin, S. W. (1998). Raman spectroscopy study of the structure of lithium and sodium ultraphosphate glasses. *J. Non Cryst. Solids* 223, 21–31. doi: 10.1016/S0022-3093(97)00347-5

Januchta, K., Youngman, R. E., Goel, A., Bauchy, M., Logunov, S. L., Rzoska, S. J., et al. (2017). Discovery of ultra-crack-resistant oxide glasses with adaptive networks. *Chem. Mater.* 29, 5865–5876. doi: 10.1021/acs.chemmater.7b00921

Kafer, D., He, M. Q., Li,J. F., Pambianchi, M. S., Feng, J. W., Mauro, J. C., and Bao, Z. N. (2013). Ultra-smooth and ultra-strong ion-exchanged glass as substrates for organic electronics. *Adv. Func. Mater.* 23, 3233–3238. doi: 10.1002/adfm.201202009

Kapoor, S., Guo, X., Youngman, R. E., Hogue, C. L., Mauro, J. C., Rzoska, S. J., et al. (2017a). Network glasses under pressure: permanent densification in modifier-free systems. *Phys. Rev. Appl.* 7:054011. doi: 10.1103/PhysRevApplied.7.054011

Kapoor, S., Januchta, K., Youngman, R. E., Guo, X., Mauro, J. C., Bauchy, M., et al. (2018). Combining high hardness and crack resistance in mixed network glasses through high-temperature densification. *Phys. Rev. Mater.* 2:063603. doi: 10.1103/PhysRevMaterials.2.063603

Kapoor, S., Lönnroth, N., Youngman, R. E., Rzoska, S. J., Bockowski, M., Jensen, L. R., et al. (2017b). Pressure-driven structural

depolymerization of zinc phosphate glass. *J. Non Cryst. Solids* 469, 31–38. doi: 10.1016/j.jnoncrysol.2017.04.011

Kapoor, S., Wondraczek, L., and Smedskjaer, M. M. (2017c). Pressure-induced densification of oxide glasses at the glass transition. *Front. Materials* 4:1. doi: 10.3389/fmats.2017.00001

Kelsey, K. E., Stebbins, J. F., Mosenfelder, J. L., and Asimow, P. D. (2009). Simultaneous aluminum, silicon, and sodium coordination changes in 6 GPa sodium aluminosilicate glasses. *Am. Miner.* 94, 1205–1215. doi: 10.2138/am.2009.3177

Kirkpatrick, R. J., and Brow, R. K. (1995). Nuclear-magnetic-resonance investigation of the structures of phosphate and phosphate-containing glasses - A review. *Solid State Nucl. Magn. Res.* 5, 9–21. doi: 10.1016/0926-2040(95)00042-O

Le Parc, R., Ranieri, V., Haines, J., Cambon, M., Cambon, O., Levelut, C., and Clément, S. (2009). *In situ* high pressure and high temperature Raman studies of (1– x)SiO_2.xGeO_2 glasses. *J. Phys. Condensed. Matter* 21:375109. doi: 10.1088/0953-8984/21/37/375109

MacKenzie, K. J. D. (2002). *Multinuclear Solid-State NMR of Inorganic Materials.* Amsterdam: Pergamon.

Mascaraque, N., Bauchy, M., Fierro, J. L. G., Rzoska, S. J., Bockowski, M., and Smedskjaer, M. M. (2017). Dissolution kinetics of hot compressed oxide glasses. *J. Phys. Chem. B* 121, 9063–9072. doi: 10.1021/acs.jpcb.7b04535

Massiot, D., Fayon, F., Capron, M., King, I., Le Calvé, S., Alonso, B., et al. (2002). Modelling one-and two-dimensional solid-state NMR spectra. *Magn. Res. Chem.* 40, 70–76. doi: 10.1002/mrc.984

Meyer, K. (1998). Characterisation of the structure of binary calcium ultraphosphate glasses by infrared and Raman spectroscopy. *Phys. Chem. Glasses* 39, 108–117.

Mosey, N. J., Muser, M. H., and Woo, T. K. (2005). Molecular mechanisms for the functionality of lubricant additives. *Science* 307, 1612–1615. doi: 10.1126/science.1107895

Muñoz, F., Montagne, L., and Delevoye, L. (2008). Influence of phosphorus speciation on the phase separation of Na_2O-B_2O_3-SiO_2 glasses. *Phys. Chem. Glasses* 49, 339–345.

Muñoz, F., Montagne, L., Delevoye, L., Durán, A., Pascual, L., Cristol, S., et al. (2006). Phosphate speciation in sodium borosilicate glasses studied by nuclear magnetic resonance. *J. Non Cryst. Solids* 352, 2958–2968. doi: 10.1016/j.jnoncrysol.2006.04.016

Muñoz, F., Pascual, L., Duran, A., Montagne, L., and Delevoye, L. (2007). Structure-property relationships in phase separated borosilicate glasses containing P_2O_5. *Phys. Chem. Glasses* 48, 296–301.

Mysen, B. O., and Frantz, J. D. (1994). Silicate melts at magmatic temperatures: *in-situ* structure determination to 1651°C and effect of temperature and bulk composition on the mixing behavior of structural units. *Contribut. Mineral. Petrol.* 117, 1–14. doi: 10.1007/BF00307725

Nelson, B., and Exarhos, G. J. (1979). Vibrational spectroscopy of cation-site interactions in phosphate glasses. *J. Chem. Phys.* 71, 2739–2747. doi: 10.1063/1.438679

Premila, M., Ravindran, T. R., Shekar, N. V. C., Abhaya, S., Rajaraman, R., Amarendra, G., et al. (2012). Effect of pressure on the structural stability of iron phosphate glass: role of trace water. *J. Non Cryst. Solids* 358, 2575–2580. doi: 10.1016/j.jnoncrysol.2012.06.005

Rao, G. V., and Shashikala, H. (2014). Optical and mechanical properties of calcium phosphate glasses. *Glass Phys. Chem.* 40, 303–309. doi: 10.1134/S1087659614030249

Rouse, G. B., Miller, P. J., and Risen, W. M. (1978). Mixed alkali glass spectra and structure. *J. Non Cryst. Solids* 28, 193–207. doi: 10.1016/0022-3093(78)90006-6

Sandler, J., Shaffer, M. S. P., Windle, A. H., Halsall, M. P., Montes-Morán, M. A., Cooper, C. A., et al. (2003). Variations in the Raman peak shift as a function of hydrostatic pressure for various carbon nanostructures: A simple geometric effect. *Phys. Rev. B* 67: 035417. doi: 10.1103/PhysRevB.67.035417

Sato, R. K., Kirkpatrick, R. J., and Brow, R. K. (1992). Structure of Li, Na metaphosphate glasses by ^{31}P and ^{23}Na MAS-NMR correlated with the mixed alkali effect. *J. Non Cryst. Solids* 143, 257–264. doi: 10.1016/S0022-3093(05)80575-7

Schneider, J., Oliveira, S. L., Nunes, L. A. O., Bonk, F., and Panepucci, H. (2005). Short-range structure and cation bonding in calcium–aluminum metaphosphate glasses. *Inorganic Chem.* 44, 423–430. doi: 10.1021/ic0499704

Schneider, J., Oliveira, S. L., Nunes, L. A. O., and Panepucci, H. (2003). Local structure of sodium aluminum metaphosphate glasses. *J. Am. Ceram. Soc.* 86, 317–324. doi: 10.1111/j.1151-2916.2003.tb00017.x

Shannon, R. D. (1976). Revised effective ionic radii and systematic studies of interatomic distances in halides and chalcogenides. *Acta Crystallogr. Sect. A.* 32, 751–767. doi: 10.1107/S0567739476001551

Shi, Y., Lonnroth, N. T., Youngman, R. E., Rzoska, S. J., Bockowski, M., and Smedskjaer, M. M. (2018). Pressure-induced structural changes in titanophosphate glasses studied by neutron and X-ray total scattering analyses. *J. Non Cryst. Solids* 483, 50–59. doi: 10.1016/j.jnoncrysol.2017.12.055

Siebers, F., Ruedinger, B., Langsdorf, A., and Heiss, M. (2014). *Glass Having Excellent Resistance Against Surface Damages and Method for the Production Thereof.* US8859079B2.

Smedskjaer, M. M., Mauro, J. C., and Yue, Y. Z. (2010). Prediction of glass hardness using temperature-dependent constraint theory. *Phys. Rev. Lett.* 105:115503. doi: 10.1103/PhysRevLett.105.115503

Smith, C. E., Brow, R. K., Montagne, L., and Revel, B. (2014). The structure and properties of zinc aluminophosphate glasses. *J. Non Cryst. Solids* 386, 105–114. doi: 10.1016/j.jnoncrysol.2013.11.042

Striepe, S., Smedskjaer, M. M., Deubener, J., Bauer, U., Behrens, H., Potuzak, M., et al. (2013). Elastic and micromechanical properties of isostatically compressed soda–lime–borate glasses. *J. Non Cryst. Solids* 364, 44–52. doi: 10.1016/j.jnoncrysol.2013.01.009

Svenson, M. N., Paraschiv, G. L., Muñoz, F., Yue, Y., Rzoska, S. J., Bockowski, M., et al. (2016). Pressure-induced structural transformations in phosphorus oxynitride glasses. *J. Non Cryst. Solids* 452, 153–160. doi: 10.1016/j.jnoncrysol.2016.08.039

Tošić, M., Nikolić, J., Grujić, S., Živanović, V., ZildŽović, S., Matijašević, S., et al. (2013). Dissolution behavior of a polyphosphate glass into an aqueous solution under static leaching conditions. *J. Non Cryst. Solids* 362, 185–194. doi: 10.1016/j.jnoncrysol.2012.11.024

van Wüllen, Züchner, L. L., Müller-Warmuth, W., and Eckert, H. (1996). $^{11}B\{^{27}Al\}$ and $^{27}Al\{^{11}B\}$ double resonance experiments on a glassy sodium aluminoborate. *Solid State Nucl. Magn. Res.* 6, 203–212.

Watson, G. H., and Daniels, W. B. (1988). Raman scattering from solid argon at high pressure. *Phys. Rev. B* 37, 2669–2673. doi: 10.1103/PhysRevB.37.2669

Yue, Y., Wondraczek, L., Behrens, H., and Deubener, J. (2007). Glass transition in an isostatically compressed calcium metaphosphate glass. *J. Chem. Phys.* 126:144902. doi: 10.1063/1.2719194

Zhang, Z., Hirao, K., and Soga, N. (1991b). Water corrosion behavior of densified glass. II. Borate glass. *J. Non-Cryst. Solids* 135, 62–66. doi: 10.1016/0022-3093(91)90443-A

Zhang, Z., Soga, N., and Hirao, K. (1991a). Water corrosion behavior of densified glass. I. Silicate glass. *J. Non-Cryst. Solids* 135, 55–61. doi: 10.1016/0022-3093(91)90442-9

Zuchner, L., Chan, J. C. C., Muller-Warmuth, W., and Eckert, H. (1998). Short-range order and site connectivities in sodium aluminoborate glasses: I. Quantification of local environments by high-resolution ^{11}B, ^{23}Na, and ^{27}Al solid-state NMR. *J. Phys. Chem. B* 102, 4495–4506. doi: 10.1021/jp980587s

Conflict of Interest Statement: RY, LM, and NL are employed by Corning Incorporated.

The reviewer MS declared a past collaboration with one of the authors MS to the handling editor.

The remaining authors declare that the research was conducted in the absence of any commercial or financial relationships that could be construed as a potential conflict of interest.